Scripta Materialia 226 (2023) 115220

Contents lists available at ScienceDirect

Scripta Materialia

journal homepage: www.journals.elsevier.com/scripta-materialia

Precipitate formation in the Fe-Al-Nb and Fe-Al-Ta systems

A. Gedsun [a,*], S. Antonov [b], T.S. Prithiv [a], M. Palm [a]

[a] Max-Planck-Institut für Eisenforschung GmbH, Max-Planck-Str. 1, D-40237 Düsseldorf, Germany
[b] National Energy Technology Laboratory, 1450 Queen Ave. SW, Albany, OR 97321, USA

ARTICLE INFO

Keywords:
Phase transformation kinetics
Heusler phases
Iron aluminides
Atom probe tomography

ABSTRACT

The composition of the metastable $L2_1$ Heusler phase in Fe_2AlX with (X = Nb, Ta) alloys has been determined by atom probe tomography (APT). It was found that the composition of $L2_1$ is off-stoichiometric in both systems, however closer to the stoichiometric composition in the Fe-Al-Ta than in the Fe-Al-Nb(-B) alloy. $L2_1$ dissolves faster and therefore the formation of the stable C14 Laves phase proceeds quicker in the Fe-Al-Nb(-B) alloy. Doping with boron does not lead to the formation of borides and only a slight enrichment of boron in the Fe-Al matrix at the grain boundary, which is covered with C14 precipitates is observed.

Iron aluminides are promising materials for structural applications at high temperatures, e.g. turbine blades, due to their excellent corrosion and wear resistance, low density, and cost-effective processing [1–4]. However, creep resistance and strength at high temperatures and ductility at room temperature still need to be improved for a wider application range. Several strengthening strategies such as solid solution hardening, strengthening by coherent or incoherent intermetallic precipitates, carbides, or borides, or increasing the ordering can be employed to further develop Fe-Al alloys [3,5-7].

A significant enhancement of creep behaviour and strength can be reached in ternary Fe-Al-X alloys through precipitation strengthening with the coherent, nano-scaled $L2_1$-ordered Heusler phase Fe_2AlX with (X = Ta, Nb, Ti, V) [8–16].

In the Fe-Al-Ti and Fe-Al-V systems, the $L2_1$ phase is thermodynamically stable and forms coherent precipitates within the disordered A2 α(Fe, Al) matrix [17,18]. These microstructures resemble those in γ/γ' in Ni-based superalloys, and the hardness, yield stress and creep resistance of Fe-Al-X (X = Ti, V) alloys can be significantly improved up to 700 °C [12,15,19].

In contrast, in the Fe-Al-Ta and Fe-Al-Nb systems, $L2_1$ is metastable and forms coherent microstructures within the B2-ordered FeAl matrix. In the Fe-Al-Ta system formation of the metastable $L2_1$ was observed for alloys within the composition range of about 20–30 at.% Al and 1.5–7 at.% Ta after annealing or creep deformation below 800 °C [13,14,20]. Due to the small size of the nano-scaled $L2_1$ precipitates, their composition could only be estimated to be about 60 at.% Fe, 20–22 at.% Ta and 15 at.% Al [13]. Upon prolonged annealing, the $L2_1$ precipitates dissolve, and the stable hexagonal C14 Laves phase nucleates. Interestingly, $L2_1$ could be still observed besides C14 after annealing at 700 °C/1000 h [14]. The precipitation of C14 can be largely influenced through aimed heat treatment [13,14], doping with boron [14], and thermomechanical processing [20]. As a result, a fine-scaled and homogeneous distribution of C14 in the matrix can be achieved.

Boron doping is known to strengthen the grain boundaries and thereby improve the strength and ductility of Fe-Al alloys [21,22]. Moreover, small amounts of boron in the matrix are suggested to affect the precipitation kinetics by providing additional nucleation sites for C14. Therefore, in previous investigations, it has been assumed that $L2_1$ precipitates do not form in boron doped Fe-Al-Ta and Fe-Al-Nb alloys, as C14 precipitates more readily in the boron doped alloys [14,23].

Similarly, in the Fe-Al-Nb system, precipitation of metastable $L2_1$ precedes the formation of C14 [9,11,24-26]. Upon annealing, the $L2_1$ coarsens and then dissolves giving way to the C14 precipitates [9,26,27]. The only measurement of the composition of the metastable $L2_1$ indicates that the composition of this phase could be quite off-stoichiometric [9]. More importantly, through the precipitation of $L2_1$, the yield stress could be improved by 50% up to temperatures of 600 °C [9] and significant hardening could be obtained [25,27]. However, in other investigations, $L2_1$ was not found in Fe-Al-Nb alloys of similar compositions [23,28,29].

Yet, knowledge on the $L2_1$ Heusler phase in Fe-Al-Nb and Fe-Al-Ta systems is limited and insufficient to completely understand its stability and relationship to the subsequent C14 Laves phase formation, which are key to achieving excellent creep properties in these promising systems.

The present investigation aims to elucidate the composition of the

* Corresponding author.
E-mail address: a.gedsun@mpie.de (A. Gedsun).

https://doi.org/10.1016/j.scriptamat.2022.115220
Received 26 September 2022; Received in revised form 5 November 2022; Accepted 28 November 2022
Available online 2 December 2022

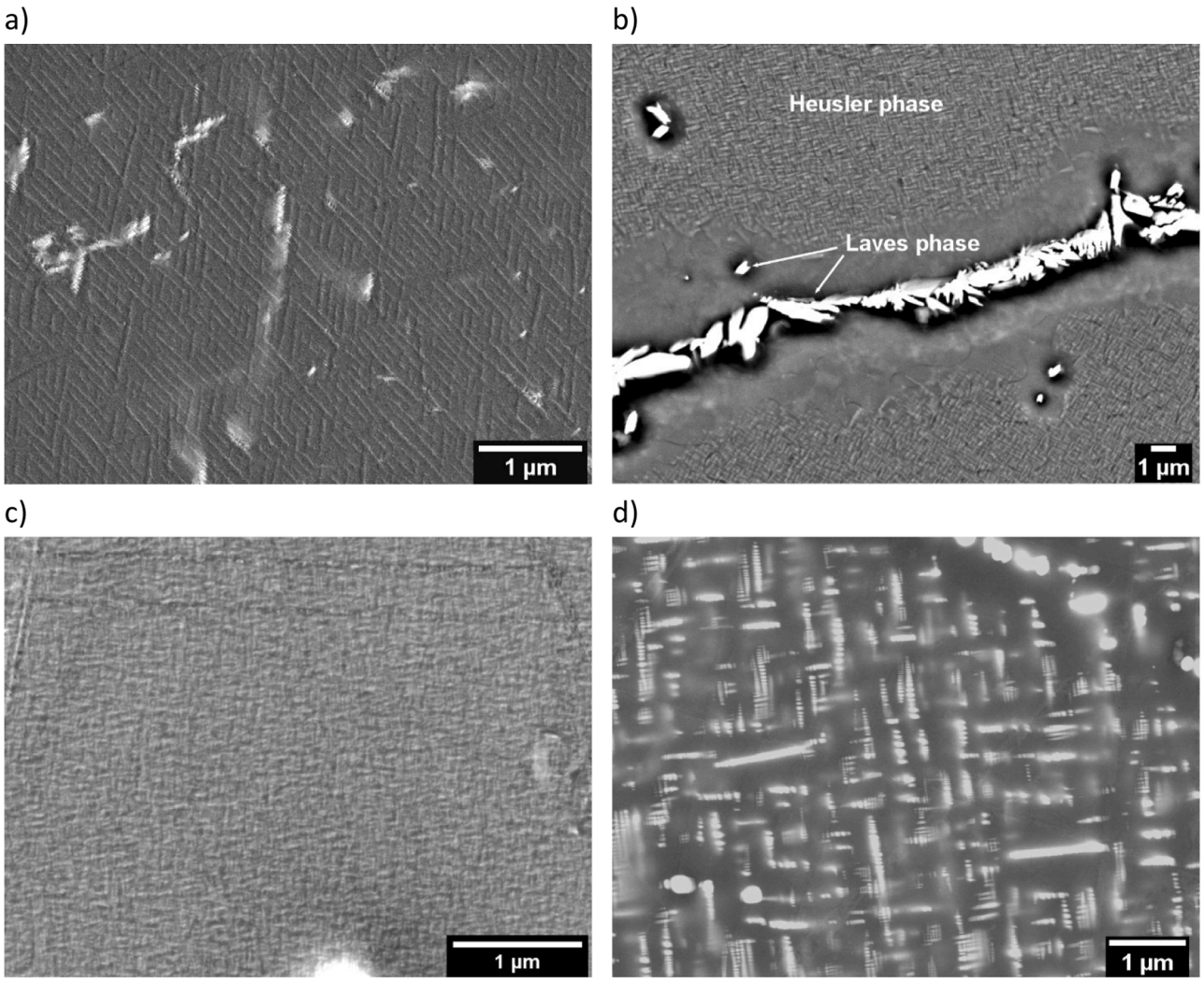

Fig. 1. Back-scattered electron (BSE) micrographs of Fe-24.4Al-2Nb-0.03B annealed at a) 600 °C/100 h, b) 700 °C/1 h [26], showing the Fe-Al matrix (grey) with interspersed $L2_1$ and Nb-rich (bright) C14 Laves phase Fe-25.9Al-1.6Ta annealed at c) 600 °C/100 h, d) 700 °C/100 h, showing the Fe-Al matrix (grey) and $L2_1$ precipitates (bright phase).

Heusler phase in the Fe-Al-Nb and Fe-Al-Ta systems and to clarify whether the kinetics of the dissolution of $L2_1$ and the formation of stable Laves C14 is analogous in both systems. The current Fe-Al-Nb alloy stems from a previous study, where the effect of doping with boron on precipitation kinetics was investigated [26], however, it has been shown that doping has no effect on phase equilibria [30].

The results obtained in this study will enable the design of more creep resistant FeAl alloys.

Fe-24.4Al-2Nb-0.03B (all compositions in at.% except when noted otherwise) was produced by vacuum induction melting under Ar from pure Fe (99.9 wt.%), Al (99.9 wt.%), Nb (99.9 wt.%) and B (99.4 wt.%). Fe-25.9Al-1.6Ta was produced from Fe (99.5 wt.%), Al (99.9 wt.%), and Ta (99.99 wt.%) by levitation melting under Ar. Both alloys were cast into copper molds of 20 mm diameter. Specimens were heat-treated in air at 600 and 700 °C for 100 h, and in the case of Fe-24.4Al-2Nb-0.03B additionally for 1 h at 700 °C, and furnace cooled. Metallographic specimens were ground and polished to 0.5 µm and additionally with oxide polishing suspension (OPS). Actual compositions of the alloys were determined by wet chemical analysis and compositions of the phases were established by wavelength-dispersive electron probe microanalysis (EPMA; Jeol JXA-8100). Quantitative analysis was performed at 15 kV and 20 nA using pure elements as standards. At least 15 to 20 measurements for each phase were performed at different areas on the specimen. Microstructures were studied by scanning electron microscopy (SEM; Zeiss LEO 1550 VP and Zeiss Merlin). Further, compositions of the phases were measured by APT (LEAP 5000 XR), operated in pulsed laser mode with a laser energy of 40 pJ, a pulse frequency of 200 kHz, a base temperature of 50 K, and detection rates up to 1.5%. Deconvolution of Fe^{2+} and Al^{1+} peaks at the 27 Da peak in the mass spectra was performed based on the natural isotopic abundancies of Fe.

The micrographs of Fe-24.4Al-2Nb-0.03B annealed at 600 °C/100 h and 700 °C/1 h show nano-scale precipitates of metastable $L2_1$ in the Fe-Al matrix (Fig.1a-b). After 600 °C/100 h only a few stable C14 precipitates formed (Fig. 1a). In contrast, a considerable amount of C14 nucleated at grain boundaries after 700 °C/1 h, and the metastable $L2_1$ dissolved in the adjacent matrix, thereby forming a precipitate-free zone along the grain boundaries (Fig. 1b) [26]. After 700 °C/100 h (not shown here) $L2_1$ precipitates were no longer observed, but instead, C14 had formed within the Fe-Al grains. In Ref. [26] it was reported that after 700 °C/10 h, the $L2_1$ phase is no longer observed in this alloy, but recent investigations of the same sample with higher resolution techniques revealed the presence of fine $L2_1$. The Fe-Al matrix is B2-ordered at 600 and 700 °C, but transforms to $D0_3$ during cooling to room temperature [30]. Therefore, the matrix has the same crystallographic structure at room temperature as the $L2_1$ precipitates, since the $D0_3$ structure of the matrix is the binary equivalent of the ternary $L2_1$

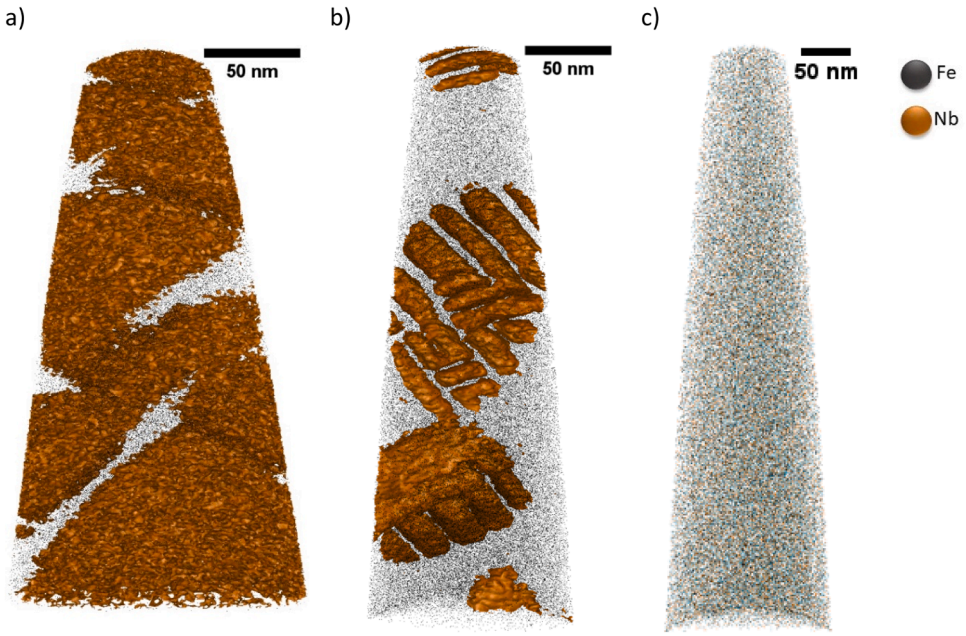

Fig. 2. APT reconstruction of Fe-24.4Al-2Nb-0.03B annealed at a) 600 °C/100 h, b) 700 °C/1 h and c) 700 °C/100 h. Fe ions are represented in black; Nb ions are represented in brown; $L2_1$ precipitates are visualized by showing an Nb isocomposition surface with a threshold of 5.5 at.% Nb (a) and 2.5 at.% Nb (b) in brown.

Table 1
Chemical composition of $L2_1$ Heusler phase precipitates and Fe-Al matrix as determined with APT in Fe-24.4Al-2Nb-0.03B. The composition of the matrix after 1000 h annealing at 700 °C determined by EPMA is given for comparison [26].

	600 °C/100 h		700 °C/1 h		700 °C/ 100 h	700 °C/1000 h (EPMA) [26]
Element	Fe-Al	L21	Fe-Al	$L2_1$	Fe-Al	Fe-Al
Fe	78.9 ± 1.1	72.4 ± 0.7	75.4 ± 0.2	63.9 ± 0.4	74.94 ± 0.01	74.4 ± 0.7
Al	20.7 ± 0.9	24.6 ± 0.7	23.2 ± 0.2	26.1 ± 0.2	24.44 ± 0.01	25.2 ± 0.6
Nb	0.4 ± 0.1	3.0 ± 0.1	1.4 ± 0.1	10.0 ± 0.2	0.62 ± 0.01	0.4 ± 0.1

Heusler phase structure. It is noted that doping with boron did not result in the formation of additional phases, e.g. borides, in agreement with a preceding study, where it was found that phase equilibria in Fe-Al-Nb are not affected by such low amounts of boron doping [30].

Micrographs of Fe-25.9Al-1.6Ta annealed at 600 and 700 °C/ 100 h are shown in Fig. 1c-d. Both specimens contain $L2_1$ precipitates. After annealing at 700 °C, the $L2_1$ precipitates coarsen significantly compared to 600 °C, in accordance to previously reported observations [14].

Comparison of the microstructures of Fe-24.4Al-2Nb-0.03B and Fe-25.9Al-1.6Ta after annealing for 100 h at 600 °C and 700 °C shows that the $L2_1$ phase dissolves much faster and that stable C14 forms earlier in the Nb containing alloy than in the Ta containing one, in accordance with previous observations [26].

To determine the composition of $L2_1$ in the Fe-Al-Nb and Fe-Al-Ta alloys, APT measurements were performed.

Reconstructions of representative APT specimens of Fe-24.4Al-2Nb-0.03B after different heat treatments are shown in Fig. 2. To highlight the $L2_1$/matrix interface, an isocomposition surface of 2.5 at.% Nb was used for the sample annealed at 600 °C/100 h and 5.5 at.% Nb for the sample annealed at 700 °C/1 h. The difference in isocomposition threshold selection arises from the compositional variation of the phases, as will be shown.

After annealing at 600 °C/100 h, rectangular shaped $L2_1$ precipitates of about 100 nm are observed (Fig. 2a). After 700 °C/1 h, rectangular shaped $L2_1$ precipitates of 10–50 nm form (Fig. 2b). Consistent with the micrographs (Fig. 1), the $L2_1$ precipitates are arranged in chains. Annealing at 600 °C/100 h leads to coarsening of the $L2_1$ precipitates due to the longer annealing time. After annealing for 100 h at 700 °C, $L2_1$ precipitates were not detected by APT (Fig. 2c), thus corroborating the microstructural observation that after 700 °C/100 h only stable C14 is present. As the C14 precipitates are rather coarse in this sample and with large interparticle spacing, they were not captured by APT within the investigated volume (Fig. 2c).

The APT determined chemical compositions of the $L2_1$ and matrix phases are given in Table 1. After 600 °C/100 h the Al content in $L2_1$ is about 25 at.%, i.e. as expected for the stoichiometric composition of Fe_2AlNb. In contrast, the Nb content is only 3 at.% and thus significantly off-stoichiometric. The $L2_1$ precipitates formed at 700 °C/1 h also show an Al content close to the one expected for the stoichiometric composition, while although the Nb content of 10 at.% is considerably higher than after 600 °C/100 h, it is still much lower than the stoichiometric composition. A frequency distribution histogram analysis (not shown here) of the ~160 million ion dataset from the 700 °C/100 h condition showed homogeneous chemical distribution. Note that the error of the composition of the sample annealed at 700 °C/100 h is much lower because it was derived from a much larger dataset. A comparison of the compositions of the matrix in the samples annealed at 700 °C (Table 1) shows that with increasing annealing time, the composition consistently shifts towards that observed in equilibrium after 1000 h [26]. The composition of C14 in Fe-24.4Al-2Nb-0.03B, annealed at 700 °C/1 h was determined as 58.3 ± 1.3 at.% Fe, 14.8 ± 0.6 at.% Al, 26.8 ± 1.6 at.% Nb by APT. For the same alloy, the composition of C14 was measured as 59.7 ± 1.3 at.% Fe, 17.0 ± 0.6 at.% Al, 23.3 ± 1.7 at.% Nb by EPMA [30] after annealing at 700 °C for 1000 h. Note that boron was not detected, in agreement with prior EPMA analysis [30].

The only available compositional measurement of metastable $L2_1$ precipitates in the Fe-Al-Nb system has been obtained by TEM-EDS [9]. After annealing Fe-25Al-2Nb (at.%) for 100 h at 650 °C,~500 nm large $L2_1$ precipitates show a composition of 24.9 at.% Al and 13.9 at.% Nb, thus resembling those determined in the present investigation, i.e. the Al content is about that of the stoichiometric composition, while the Nb content is considerably lower. The considerably lower Nb contents in $L2_1$ than the expected stoichiometric composition of Fe_2AlNb is also

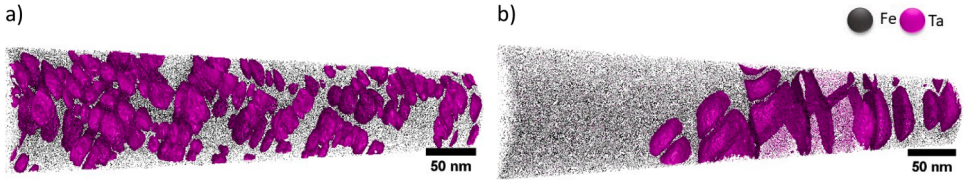

Fig. 3. APT reconstruction of Fe-25.9Al-1.6Ta annealed a) 600 °C/100 h and b) 700 °C/100 h. Fe ions are represented in black, Ta ions are represented in purple; the Ta isocomposition-surface with the threshold of 10 at.% Ta, in purple, delineates the Heusler phase from the matrix.

Table 2
Chemical compositions of the $L2_1$ Heusler phase precipitates and the Fe-Al matrix, as determined with APT in Fe-25.9Al-1.6Ta annealed at 600 and 700 °C for 100 h; the composition of the matrix of 25.7Al-1.6Ta after 1000 h annealing at 700 °C determined by EPMA is given for comparison [14].

	600 °C/100 h		700 °C/100 h		700 °C/1000 h (EPMA) [14]
Element	Fe-Al	$L2_1$	Fe-Al	$L2_1$	Fe-Al
Fe	75.7 ± 0.2	55.6 ± 0.5	75.3 ± 0.4	54.9 ± 0.4	74.8 ± 0.3
Al	23.5 ± 0.1	27.2 ± 0.3	23.6 ± 0.4	26.3 ± 0.3	24.6 ± 0.3
Ta	0.8 ± 0.2	17.2 ± 0.4	1.1 ± 0.1	18.8 ± 0.3	0.54 ± 0.07

supported by calculations. In a combined CVM and DFT study, Eleno et al. [31] calculated the metastable Fe-Al-Nb isothermal section at 627 °C (900 K). According to these *ab initio* calculations, metastable $L2_1$ occurs with Nb contents between 2 and 25 at.% for 25 at.% Al at that temperature, in accordance with compositions measured in [9] and in the present investigation.

Reconstructions of the APT needles of Fe-25.9Al-1.6Ta annealed at 600 °C and 700 °C for 100 h are shown in Fig. 3. The $L2_1$ precipitates have a rectangular morphology and are arranged in chains, similar to the SEM observations (Fig.1c-d), with a particle spacing of around 5–10 nm (Fig. 3). After annealing at 600 °C, the precipitates are ~10–20 nm large, while after annealing at 700 °C they are somewhat coarser (~50 nm). After 600 °C/100 h the precipitates are finer and more homogeneously distributed than after 700 °C/100 h, which could be associated with the quicker coarsening at higher temperatures.

Although a composition range for the formation of metastable $L2_1$ in the Fe-Al-Ta system has been reported [14], the composition of $L2_1$ itself, however, has not been reported. The APT determined composition of the $L2_1$ and Fe-Al matrix in both samples is given in Table 2.

The Al contents of 26–27 at.% are again close to the stoichiometric composition of the Heusler phase. With 17–19 at.% Ta the composition of $L2_1$ is closer to the stoichiometric composition than in the Fe-Al-Nb (-B) alloy. Comparison of the matrix composition to that of a similar composition alloy [14] (Table 2) shows that after annealing at 700 °C for 100 h, the Ta content is still considerably higher than after 1000 h. For the latter alloy it was shown that even after 1000 h some residual metastable $L2_1$ precipitates are present. In contrast, in the Fe-Al-Nb-B alloy, there is little difference in the composition of the matrix after annealing for 100 or 1000 h at 700 °C and $L2_1$ precipitates are not observed past 100 h. This confirms that the metastable Heusler phase persists longer in the Fe-Al-Ta than in the Fe-Al-Nb-B alloy.

Boron peaks were not detected in the APT mass spectra of the Fe-Al matrix or $L2_1$ in Fe-24.4Al-2Nb-0.03B. Additionally, borides were also not found. It could therefore be assumed that boron segregates to grain boundaries, which are mostly covered with C14 precipitates. Therefore, APT samples were extracted from a grain boundary. Fig. 4 shows the interface between a grain boundary C14 and the surrounding Fe-Al matrix (Fig. 4a) and the composition profile perpendicular to the interface (Fig. 4b). The concentration profile in Fig. 4b indicates a slight boron enrichment of up to 0.1 at.% in the Fe-Al matrix adjacent to the grain boundary. As boron diffuses very fast, a homogeneous distribution can be expected at 700 °C. Then segregation to grain boundaries occurs during cooling, which could explain why boron doping does not accelerate the formation of C14 in the present alloy, contrary to previous observations [14,23].

In summary, we explored the metastable $L2_1$-ordered Heusler phase in a Fe-Al-Nb alloy doped with boron and a Fe-Al-Ta alloy. The Al content in the $L2_1$ was close to the stoichiometric composition (~25 at.%) in both alloys. Interestingly, the Nb content in the $L2_1$ phase of the

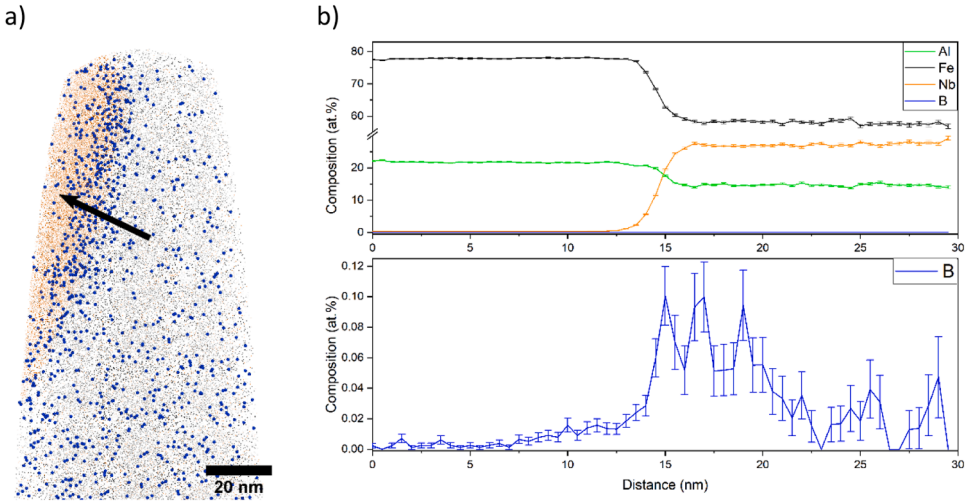

Fig. 4. a) APT reconstruction of the grain boundary, covered with the Nb-rich C14 Laves phase in Fe-24.4Al-2Nb-0.03B, annealed at 700 °C for 1 h. Fe ions are represented in black, the Nb ions in brown, and the boron ions in blue. b) Proxigram across the interface between the Fe-Al matrix and the grain boundary, covered with C14, showing the concentration profiles of Fe, Al, Nb, and B. c) Enlarged concentration profile for B.

Fe-Al-Nb alloy, was far off-stoichiometric, whereas, in the Fe-Al-Ta alloy, the Ta content in the $L2_1$ was much closer to the stoichiometric composition. Increasing the temperature from 600 to 700 °C results in coarsening of the $L2_1$ in the Fe-Al-Ta alloy, while in the Fe-Al-Nb(-B) alloy, the $L2_1$ rapidly dissolves, giving way to the stable C14 Laves phase precipitates. The change from metastable $L2_1$ to stable C14 occurs at considerably shorter times in the Fe-Al-Nb(-B) alloy than in the Fe-Al-Ta alloy. The slower dissolution of $L2_1$ and the later formation of C14 in Fe-Al-Ta alloys can be correlated with the less off-stoichiometric composition of $L2_1$ in Fe-Al-Ta, and the slower diffusion of Ta in FeAl, compared to Nb [32,33]. As the coherent precipitates contribute sifnificantly to the strength of the alloys, the inferior stability of $L2_1$ explains why lower creep resistance (not yet published work) and yield strength [26] are observed in Fe-Al-Nb alloys, compared to Fe-Al-Ta alloys. The boron doping of the Fe-Al-Nb alloy did not result in the formation of borides, however, a slight enrichment in the Fe-Al matrix near grain boundaries, and particularly at the grain boundary C14 interface.

Declaration of Competing Interest

None.

Acknowledgments

The authors would like to thank Michael Kulse and Frank Rütters for alloy fabrication, Jürgen Wichert for heat treatments and Irina Wossack for EPMA measurements. Partial financial support by the Federal Ministry for Economic Affairs and Energy through grant 0324317C is gratefully acknowledged.

Supplementary materials

Supplementary material associated with this article can be found, in the online version, at doi:10.1016/j.scriptamat.2022.115220.

References

[1] D. Hardwick, G. Wallwork, Iron-aluminium base alloys: a review of their feasibility as high temperature materials, Rev. High-Temp. Mater 4 (1978) 47–74.
[2] C.G. McKamey, Iron Aluminides, in: N.S. Stoloff, V.K. Sikka (Eds.), Physical Metallurgy and Processing of Intermetallic Compounds, Chapman Hall, New York, 1996, pp. 351–391.
[3] D.G. Morris, M.A. Muñoz-Morris, Recent developments toward the application of iron aluminides in fossil fuel technologies, Adv. Eng. Mater. 13 (2011) 43–47.
[4] M. Palm, F. Stein, G. Dehm, Iron aluminides, Annu. Rev. Mater. Res. 49 (2019) 297–326.
[5] A. Schneider, L. Falat, G. Sauthoff, G. Frommeyer, Constitution and microstructures of Fe–Al–M–C (M=Ti, V, Nb, Ta) alloys with carbides and Laves phase, Intermetallics 11 (2003) 443–450.
[6] M. Palm, Concepts derived from phase diagram studies for the strengthening of Fe–Al-based alloys, Intermetallics 13 (2005) 1286–1295.
[7] M. Palm, Fe-Al materials for structural applications at high temperatures: current research at MPIE, Int. J. Mater. Res. 100 (2009) 277–287.
[8] G. Culbertson, C.S. Kortovich, Development of Iron Aluminides, AF Wright Aeronautical Laboratories, 1986. Report AFWAL-TR-85-4155, 1-149.
[9] D.M. Dimiduk, M.G. Mendiratta, D. Banarjee, H.A. Lipsitt, A structural study of ordered precipitates in an ordered matrix within the Fe–Al–Nb system, Acta Metall. 36 (1988) 2947–2958.
[10] K. Brzakalik, J.E. Frackowiak, A Mössbauer and structural study of disordered alloys $Fe_{3-x}Ti_xAl$ ($0 < x < 1$), Nukleonika 48 (2003) 13–16.
[11] D.G. Morris, M.A. Muñoz-Morris, L.M. Requejo, C. Baudin, Strengthening at high temperatures by precipitates in Fe–Al–Nb alloys, Intermetallics 14 (2006) 1204–1207.
[12] R. Krein, M. Palm, M. Heilmaier, Characterization of microstructures, mechanical properties, and oxidation behavior of coherent A2 + $L2_1$ Fe-Al-Ti, J. Mater. Res. 24 (2009) 3412–3421.
[13] D.D. Risanti, G. Sauthoff, Microstructures and mechanical properties of Fe–Al–Ta alloys with strengthening Laves phase, Intermetallics 19 (2011) 1727–1736.
[14] P. Prokopčáková, M. Švec, M. Palm, Microstructural evolution and creep of Fe–Al–Ta alloys, Int. J. Mater. Res. 107 (2016) 396–405.
[15] L. Senčekova, M. Palm, J. Pešička, and J. Veselý, Microstructures, mechanical properties and oxidation behaviour of single-phase Fe3Al (D03) and two-phase α-Fe,Al (A2) + Fe3Al (D03) Fe–Al–V alloys, Intermetallics, 73 (2016) 58–66.
[16] P.A. Ferreirós, P.R. Alonso, P.H. Gargano, P.B. Bozzano, H.E. Troiani, A. Baruj, G. H. Rubiolo, Characterization of microstructures and age hardening of $Fe_{1-2x}Al_xV_x$ alloys, Intermetallics 50 (2014) 65–78.
[17] M.G. Mendiratta, S.K. Ehlers, H.A. Lipsitt, $D0_3$-B2-α phase relations in Fe-Al-Ti alloys, Metall. Trans. A 18 (1987) 509–518.
[18] P.Z. Zhao, T. Kozakai, T. Miyazaki, Phase separation into A2 + $D0_3$ two phases in Fe-Al-V ternary ordering alloys, J. Japan Inst. Metals 53 (1989) 266–272.
[19] P.A. Ferreirós, P.R. Alonso, G.R. Gomez, G.H. Rubiolo, Impact toughness transition temperature of ferritic Fe-Al-V alloy with strengthening Fe_2AlV precipitates, Mater. Sci. Eng. A 706 (2017) 136–141.
[20] P. Hanus, E. Bartsch, M. Palm, R. Krein, K. Bauer-Partenheimer, P. Janschek, Mechanical properties of a forged Fe–25Al–2Ta steam turbine blade, Intermetallics 18 (2010) 1379–1384.
[21] M.A. Crimp, K. Vedula, Effect of boron on the tensile properties of B2 FeAl, Mater. Sci. Eng. 78 (1986) 193–200.
[22] C.T. Liu, C.G. McKamey, E.H. Lee, Environmental effects on room-temperature ductility and fracture in Fe_3Al, Scripta Metallurgica et Materialia 24 (1990) 385–390.
[23] S.A. Azmi, A. Michalcová, L. Senčekova, M. Palm, Microstructure and mechanical properties of Fe–Al–Nb–B alloys, MRS Adv. 2 (2017) 1353–1359.
[24] D.G. Morris, M.A. Muñoz-Morris, The stress anomaly in FeAl–Fe_3Al alloys, Intermetallics 13 (2005) 1269–1274.
[25] D. Morris, L. Requejo, M. Munozmorris, Age hardening in some Fe–Al–Nb alloys, Scr. Mater. 54 (2006) 393–397.
[26] A. Gedsun, F. Stein, M. Palm, Development of new Fe–Al–Nb(–B) alloys for structural applications at high temperatures, MRS Adv., 6 (2021) 176–182.
[27] D.G. Morris, L.M. Requejo, M.A. Muñoz-Morris, A study of precipitation in $D0_3$ ordered Fe-Al-Nb alloy, Intermetallics 13 (2005) 862–871.
[28] M. Palm, Phase equilibria in the Fe corner of the Fe–Al–Nb system between 800 and 1150 °C, J. Alloys Compd. 475 (2009) 173–177.
[29] O. Prymak, F. Stein, Solidification and high-temperature phase equilibria in the Fe–Al-rich part of the Fe–Al–Nb system, Intermetallics 18 (2010) 1322–1326.
[30] A. Gedsun, F. Stein, M. Palm, Phase equilibria in the Fe-Al-Nb(-B) system at 700 °C, J. Phase Equil. Diffus. (2022) available online.
[31] L.T.F. Eleno, L.A. Errico, P.G. Gonzales-Ormeño, H.M. Petrilli, C.G. Schön, Ordering phase relationships in ternary iron aluminides, Calphad 44 (2014) 70–80.
[32] A.A. Coelho, TOPAS and TOPAS-Academic: an optimization program integrating computer algebra and crystallographic objects written in C++, J. Appl. Crystallogr. 51 (2018) 210–218.
[33] R. Bügel, H.J. Maier, T. Niendorf, Handbuch Hochtemperatur-Werkstofftechnik, 4th ed., Viewer + Teubner Verlag | Springer Fachmedien Wiesbaden GmbH, 2011.